Lattice Thermal Conductivity and Phonon Transport Properties of Monolayer Fluorographene

Author: Seungbin Han[1,2*], Dongkyu Lee[1], Sungwoo Lee[1,2], Gun-Do Lee[1,2], Sangyeop Lee[3], Hyejin Jang[1,2*]

[1]Department of Materials Science and Engineering, Seoul National University, Seoul 08826, Republic of Korea

[2]Research Institute of Advanced Materials, Seoul National University, Seoul 08826, Republic of Korea

[3]Department of Mechanical Engineering and Materials Science, University of Pittsburgh, Pittsburgh, Pennsylvania 15261, USA

Corresponding Author: seungbin_h@snu.ac.kr and hjang@snu.ac.kr

Abstract

Successful design of thermal management materials requires not only high thermal conductivity but also appropriate electrical and mechanical properties. Fluorographene, a fluorinated graphene-derivative, is expected to feature both high thermal conductivity and electrical insulation at the same time, making it an emerging material for thermal management in electronic devices. However, the phonon transport properties of monolayer fluorographene have not been fully understood. In this paper, we investigated the lattice thermal conductivity and phonon transport properties of monolayer fluorographene using first-principles calculation. The solution of the fully linearized phonon Boltzmann transport equation gives the lattice thermal conductivity of monolayer fluorographene as 145.2 W m^{-1} K^{-1} at 300 K, which is about twenty times smaller than that of monolayer graphene. We systematically compared the phonon transport properties of all the phonon modes in graphene and fluorographene in terms of phonon vibration polarization. The significantly reduced thermal conductivity of fluorographene can be attributed to the lowering of both the single-mode lifetime of the flexural acoustic phonons and the group velocities of all acoustic phonons. We concluded that the breaking of in-plane mirror symmetry and the weaker in-plane chemical bonds induced by the addition of fluorine atoms led to the suppression of lattice thermal conductivity of monolayer fluorographene. Finally, we investigated the anomalously large contribution of optical phonons to the thermal transport process in fluorographene, where the large group velocities of selected optical phonons were derived from the in-plane acoustic modes of graphene. Our work provides a new approach to study the influence of chemical functionalization on the phonon structure and to explore graphene-derived thermal management materials.

I. Introduction

Due to the rapid downsizing of modern electronic and energy devices, the heat generation per unit area is surging, and, accordingly, strategies to control the heat are of the upmost importance. For thermal management materials, not only high thermal conductivities but also appropriate electrical and mechanical properties that suit the respective device environments are required. For instance, electrical insulation may be required in electronic devices where the leakage of electrical current may affect the performance of the device. With respect to the fabrication or the durability of devices, the viscosity or flexibility of thermal interface materials may enhance the long-term performance.

Graphene and graphite have long attracted attention of in the field of thermal management due to their high thermal conductivity and large anisotropy in thermal transport. The thermal conductivity of free-standing monolayer graphene was measured to be within the large range of 1,800-5,300 W m^{-1} K^{-1},[1-3] which is the highest among all known materials so far. The high thermal conductivity is also present in few-layer graphene and bulk graphite systems which still feature ~70% of the monolayer thermal conductivity.[4] Based on their high thermal conductivity, applications of graphene and graphite systems for thermal management, such as heat spreaders or fillers in thermal interfacial materials, has also been under research.[5,6] However, the graphene-based systems always show a certain amount of electrical conduction and cannot be utilized for environments requiring electrical insulation in the thermal management material.

To utilize the high thermal conductivity of graphene and additionally incorporate an electrically insulating characteristic, fluorographene has gained great attention as a promising candidate.[7-11] Fluorographene is a fluorinated derivative of graphene, where one fluorine atom forms a chemical bond with a carbon atom perpendicularly to the graphene plane. The position of fluorine atoms alternates above or below the carbon atoms, which induces buckling in the two-dimensional (2D) carbon plane. Monolayer fluorographene is also known as the only halogenated graphene that maintains the stoichiometric one-to-one ratio between the carbon and the halogen atoms.[12] Due to the sp^3 covalent bonding character, fluorographene features negligible electrical conduction with an electronic band gap about 3.8 eV,[13] as opposed to the semi-metallic character of graphene. This helps conducting heat and insulating electricity at the same time. Thanks to these attractive physical properties, fluorographene has emerged as a prospective thermal management material for electronic devices, and the applications of fluorographene, especially in the form of composite materials,[10,11] have been actively explored and showing promising performance.

Still, the thermal transport properties of pristine fluorographene have not been fully understood. There is a limited number of studies that investigated the thermal conductivity of monolayer fluorographene using computational methods. In 2012, Huang et al.[14] calculated the lattice thermal conductivity of fully and partially fluorinated graphene using non-equilibrium molecular dynamics and proposed that the thermal conductivity of pristine monolayer fluorographene is 35% of that of monolayer graphene, which is about 850 W m^{-1} K^{-1} near 300 K. Although they analyzed the thermal conductivity according to the fluorine coverage and the orderedness of fluorination pattern, their approach was more focused on the macroscopic engineering of functionalization, failing to explain the distinct phonon characteristics of fluorographene. Additionally, two articles from the same research group reported the lattice thermal conductivity of monolayer fluorographene using first-principle calculations in 2014 and 2015, respectively, both of which predicting about 260 W m^{-1} K^{-1}.[15,16] Fugallo et al. explored the phonon thermal conductivity of graphene and its multilayer counterparts as well as functionalized form, e.g., graphane (hydrogenated graphene) and grafane (fluorographene). Cepellotti et al. examined the importance of normal scattering of phonons in 2D materials, such as graphene, functionalized graphene, boron nitride, and molybdenum disulphide. Although the authors obtained the exact solution of the phonon Boltzmann transport equation to capture the collective phonon picture in 2D materials, neither of them investigated how the crystal and chemical structures of a specific 2D material intrinsically influence the phonon transport properties, leaving thermal transport mechanism of fluorographene undiscovered. Meanwhile, a single experimental study, so far, investigated the in-plane and out-of-plane thermal conductivity of multilayer fluorographene, ranging from few-layer to 100 nm thick smaples,[17] but the samples were only partially fluorinated, failing to capture the intrinsic phonon thermal transport in fluorographene.

In this work, we investigated the lattice thermal conductivity and the phonon transport properties of monolayer

fluorographene using first-principle calculations, and systematically compared these properties with those of monolayer graphene. Density functional theory (DFT) and the phonon Boltzmann transport equation are known as the optimal tools to reproduce the lattice thermal conductivity with highly accurate phonon transport picture. Nevertheless, they often fail to predict the properties of 2D materials due to the large anharmonicity of phonons in the 2D systems. The iterative method, the most widely used method to solve the phonon Boltzmann transport equation, often yields diverging solutions for systems with frequently repopulated phonons, typically 2D systems such as graphene.(18) To deal with this hardship, we solved the fully linearized phonon Boltzmann transport equations by the direct diagonalization of the phonon collision matrices and obtained the lattice thermal conductivity of infinitely large monolayer fluorographene to be 145.2 W m^{-1} K^{-1} at 300 K, which is smaller than the values previously reported using first-principle calculations.[15,16] We found that the ZA phonons show a considerably suppressed contribution to the in-plane thermal conductivity of fluorographene compared to the contributions of both the LA and TA phonons and the optical phonons. Thorough investigation on the intrinsic phonon properties, such as scattering lifetime and group velocities, were conducted to correlate the effect of crystal structure and chemical bonds to the phonon transport phenomena. Lastly, selected optical phonon modes turned out to exhibit an anomalously large contribution to the thermal transport process, which is consistent with the prior arguments about the phonon transport properties of functionalized graphene systems by Lindsay and Kuang.[18] We provided further analysis on the vibrational properties of the certain phonon modes to find the origin of the high group velocity of optical phonons in monolayer fluorographene.

II. Calculation methods

All DFT and density functional perturbation theory (DFPT) calculations were performed using the Vienna *ab initio* simulation package (VASP).[19] Here, the generalized gradient approximation of Perdew, Berke, and Ernzerhof[20] (GGA-PBE) were chosen for the exchange-correlation functional, and projector augmented wave (PAW) pseudopotentials[21] were utilized with a plane-wave cutoff energy of 650 eV for both monolayer graphene and fluorographene. We conducted DFT calculations for geometric optimization of the primitive unit cells of monolayer graphene and fluorographene. The convergence limit to break the iteration of ionic relaxation was set as 10^{-6} eV. The electronic-structure calculations used Γ-centered Brillouin zone sampling of 24 × 24 × 1 k-points for both materials. Here, we inserted a 30 Å vacuum layer between monolayers, preventing the interlayer interaction from entering the calculation. The calculated lattice constants agree well with the reported values,[22,23] within the difference of 1% for both materials.

Subsequently, the second- and third-order force constants were calculated with the optimized structures. The second-order force constants were calculated using DFPT and were extracted using the PHONOPY package[24]. These force constants construct the dynamical matrix, which are eventually diagonalized to yield the phonon dispersion relation and harmonic properties. We also post-processed the second order force constants using the HIPHIVE package[25] to ensure that they obey the translational and rotational symmetries of the crystal system. This treatment particularly helps correctly illustrate the quadratic dispersion of the flexural acoustic (ZA) phonon modes of 2D systems. Meanwhile, the third-order force constants were calculated with finite displacement method, where the thirdorder.py script of the SHENGBTE package[26,27] was used to generate displaced supercells and reconstruct the force constants. Up to the tenth-nearest neighbor was considered while calculating the third-order force constants of both monolayer graphene and fluorographene. The electronic structures of supercells with sizes of 8 × 8 × 1 unit cells were optimized with 3 × 3 × 1 k-points for the calculation of second- and third-order force constant of the two systems.

Finally, the lattice thermal conductivities of monolayer graphene and fluorographene were calculated, using both the single-mode relaxation time approximation (RTA)[28] and the fully linearized phonon Boltzmann transport equation (LBTE), also known as the Peierls-Boltzmann transport equation. We utilized the PHONO3PY package[24,28] in both cases. The LBTE was solved by directly diagonalizing the phonon collision matrices[28,29] in order to yield the accurate lattice thermal conductivity for 2D systems featuring large phonon anharmonicity.[30] Within both calculation schemes, we solved the phonon Boltzmann transport equation with the tetrahedron method[31] on a 100 × 100 × 1 mesh (884 irreducible points) to sample the phonons in the Brillouin zone. The interlayer distances are specified to be 3.35 and 5.96 Å for the monolayer graphene and fluorographene,

respectively, taken from the experimental values in order to yield the lattice thermal conductivities of 2D materials.[23,32]

III. Results and discussions

1. Crystal structures

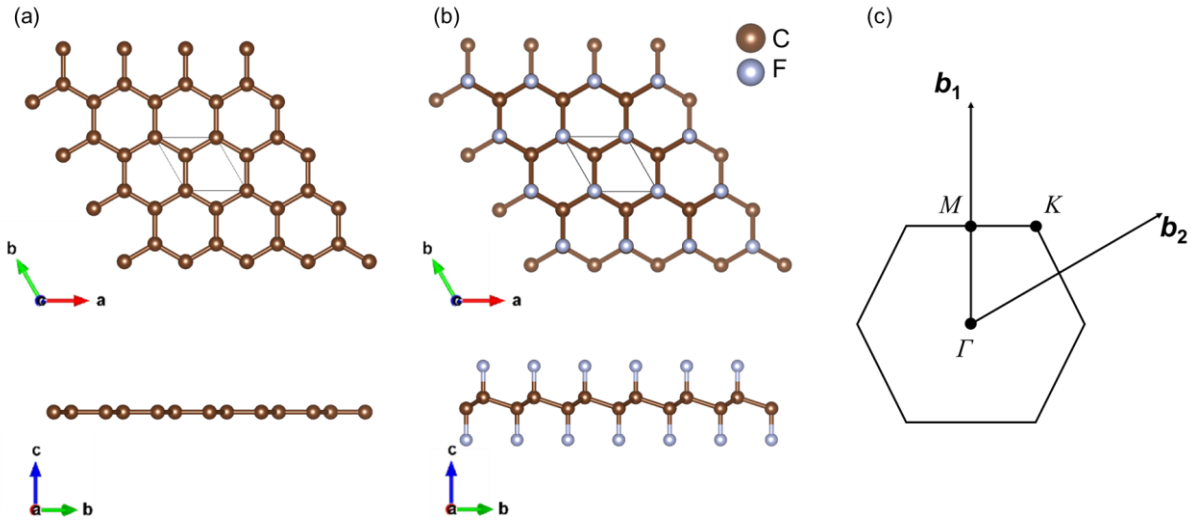

Figure 1. Top and side views of supercells of (a) monolayer graphene and (b) fluorographene, where brown and purple circles indicate carbon and fluorine atoms, respectively (c) First Brillouin zone, reciprocal lattice vectors (b_1 and b_2), and high symmetry points (Γ, K, M) of the two-dimensional hexagonal honeycomb lattice.

Table I. Crystallographic space group, lattice constants, planar density, and length and second-order force constant of the carbon-carbon bond in monolayer graphene and fluorographene in their optimized structures.

Material	Space group (No.)	In-plane lattice constant (a, Å)	Planar density (10^{-9} g cm^{-2})	Bond length (C-C, Å)	2nd order Force constant ($\|\Phi\|_{C-C}$, eV Å^{-2})
Graphene	P6/mmm (191)	2.468	75.61	1.425	27.42
Fluorographene	P-3m1 (164)	2.608	176.39	1.577	14.86

Figure 1 and Table I represent the optimized lattice structures and chemical bond features of monolayer graphene and fluorographene. Whereas monolayer graphene features a hexagonal honeycomb lattice with two bases, monolayer fluorographene possesses four basis atoms, two carbon and two fluorine atoms, in its primitive unit cell. The addition of two fluorine basis atoms induces buckling in the carbon plane (Figure 1(b)) and alters the one-atom-thick crystal structure of graphene (P6/mmm) into a less symmetrical trigonal space group(P-3m1). In terms of electronic structure, this structural change may arise from the itinerant 2p electrons of graphene being captured by the additional fluorine atoms, transitioning from the sp^2 to sp^3 chemical bond. This transition also changes the length and strength of the atomic bonds constituting the carbon plane, as can be seen from Table 1. The length of the in-plane C-C bonds is 1.577 Å in fluorographene and larger than 1.425 Å in graphene, implying weaker bond strength along the pathway of phonon transport. In fact, we investigated the norm of the second-order force constants about the C-C bonds from the dynamical matrix to find the actual bond strength in each system, and found that the force constant in graphene (27.42 eV Å^{-2}) is almost twice as large as that of fluorographene (14.86 eV Å^{-2}). The crystal symmetry and the bond strength affect the phonon scattering lifetime

and group velocity, respectively, which is discussed in the following sections.

2. Phonon dispersion and polarization

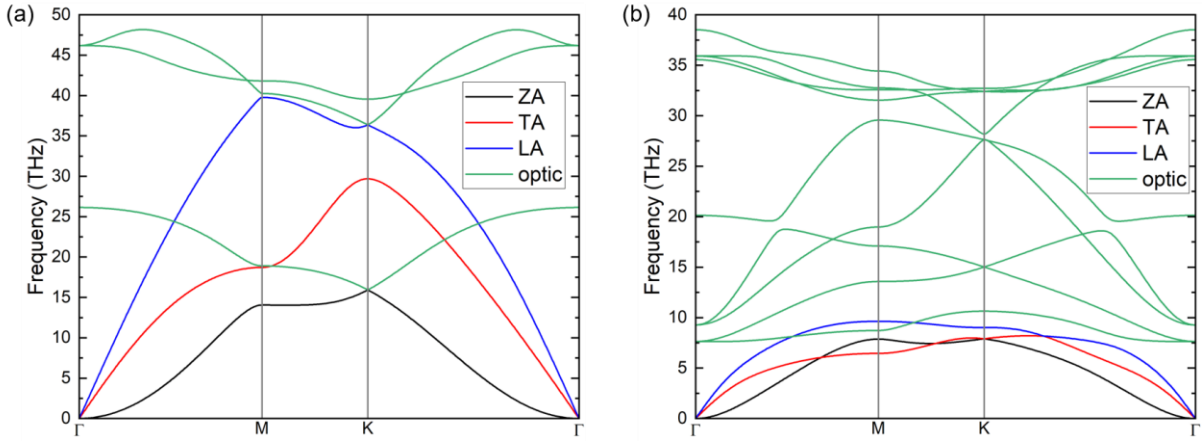

Figure 2. Phonon dispersions of (a) monolayer graphene and (b) fluorographene along the high symmetry axes. The colors represent the phonon polarization, or branch, of the lattice vibration. For both materials, flexural acoustic (ZA, black), transverse acoustic (TA, red), longitudinal acoustic (LA, blue), and optical modes (green) are specified.

The phonon dispersions of monolayer graphene and fluorographene are illustrated in Figure 2, where the polarizations of respective phonon modes are also indicated: the flexural acoustic (ZA) modes are colored in black, transverse acoustic (TA) modes in red, longitudinal acoustic (LA) modes in blue, and optical modes in green. It should be noted that the ZA branches in both cases exhibit quadratic dispersions near the Γ point, which are the most remarkable feature in the thermal transport properties of 2D materials. The phonon dispersions agree well in all frequency region with the previously reported calculation results in both graphene and fluorographene.[33,34]

Monolayer graphene and fluorographene has six and twelve phonon branches, respectively, which are three-times the number of their basis atoms. As a convention, all phonon branches excluding those having zero energy at the zone center are classified as optical; thus, monolayer graphene has three optical branches, and fluorographene has nine. Apparently, the acoustic branches are more energetically suppressed in fluorographene compared to graphene. The frequencies of acoustic phonons in monolayer fluorographene always stay below 10 THz, whereas the graphene counterparts surge at most 40 THz, which corresponds to the LA phonon at the M point. In contrast, the optical branches of fluorographene occupy the large frequency range of 7.6-38.5 THz, and a few of them show steep phonon dispersions, signifying large group velocity of phonons. These peculiar optical phonon modes, although labeled as optical modes, may largely contribute to the total thermal transport process, whose physical origin will be further explained in the following section about phonon polarization.

3. Lattice thermal conductivity

Figure 3 shows the calculated lattice thermal conductivities (κ) of monolayer graphene and fluorographene as a function of temperature and system size. In Figure 3(a), only the three-phonon and isotope scatterings were incorporated in the calculation of lattice thermal conductivity to exclude the influence of boundary scattering due to the finite sizes of samples. At 300 K, the thermal conductivities of monolayer graphene and fluorographene were predicted to be 2,868.6 and 145.2 W m^{-1} K^{-1}, respectively, when solved from the LBTE approach. The LBTE result suggests that monolayer fluorographene shows about 20 times lower lattice thermal conductivity than that

of graphene at this temperature. This large difference in lattice thermal conductivity is unexpected when considering only the atomic mass density and bond strength of the individual systems. Meanwhile, the RTA predicts the lattice thermal conductivities of graphene and fluorographene to be 472.3 and 112.2 W m^{-1} K^{-1}, respectively. The RTA and LBTE solutions differ largely in both material systems at the entire temperature range of 100-800 K. Compared to the RTA results, the LBTE solution yielded a six-fold increase in graphene, and about a 30% increase in fluorographene. In conventional 3D materials, the full LBTE calculation alters only less than 10% of the room-temperature thermal conductivity compared to the RTA solution.[35] In contrast, in our results for both graphene and fluorographene, the discrepancies between RTA and LBTE solutions are significantly larger than the typical 3D materials. The failure of the single-mode phonon picture suggests the breakdown of the diffusive phonon transport behavior and the presence of hydrodynamic phonon transport.[15,16]

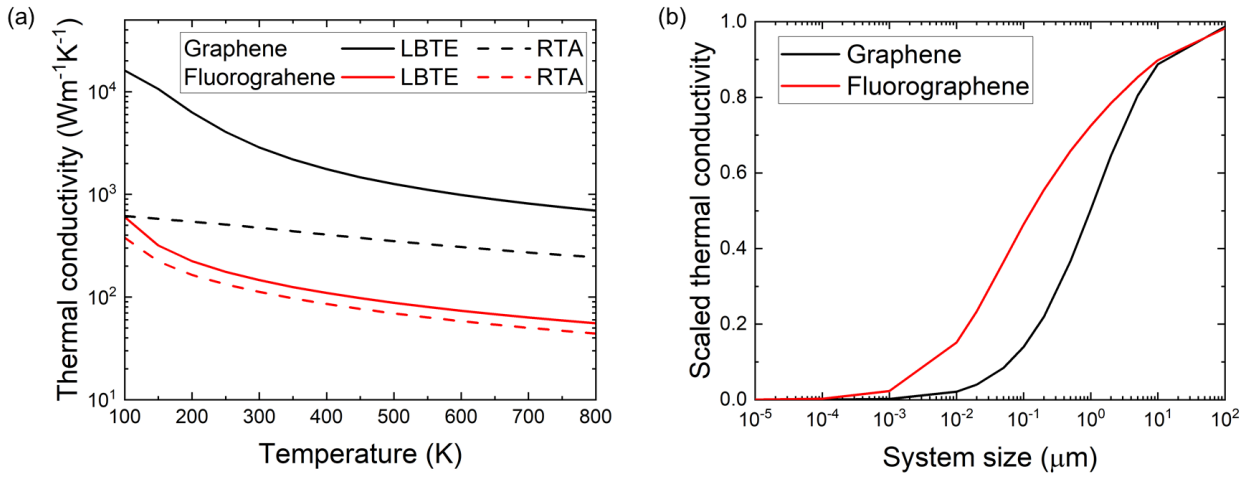

Figure 3. (a) Lattice thermal conductivities of single-crystal monolayer graphene (black) and fluorographene (red) samples, calculated by the direct diagonalization of phonon collision matrix (solid line) and the single mode relaxation time approximation (dotted line). (b) The calculated scaled lattice thermal conductivity of samples at 300 K with finite system size.

Meanwhile, it can be inferred that the thermal transport in monolayer fluorographene is less affected by the system size than graphene is, as illustrated in Figure 3(b). The scaled thermal conductivity, κ_{scale}, is defined as the thermal conductivity of the given crystal size, κ_L, divided by its value for infinitely large system size, $\kappa_{L\to\infty}$:

$$\kappa_{\text{scale}} = \kappa_L/\kappa_{L\to\infty}.$$

where κ_L incorporates the effect of boundary scattering

$$1/\tau_{\text{boundary},\lambda} = v_{g,\lambda}/L$$

while calculating the scattering rate of individual phonon mode λ with Mattiessens's rule.[15] Here, we calculated the scaled thermal conductivity at 300 K. This parameter, typically dependent on the rate of boundary scattering of the system, shows how largely the thermal conductivity of certain material is affected by the system size of the sample. The calculation of scaled thermal conductivities shows that monolayer fluorographene recovers half of its infinite-crystal lattice thermal conductivity when its system sizes are larger than 100 nm, whereas graphene requires system size larger than 1 μm. This result suggests that the thermal conductivity of monolayer fluorographene is less impacted by the system size than that of graphene; thus, may feature more tunability in

submicro-scaled systems.

Although the temperature-dependent lattice thermal conductivity of monolayer fluorographene follows a similar trend to the previously reported calculation results,[15,16] our calculated result is scaled almost half in magnitude compared to the prior reports. The difference in the magnitude of thermal conductivity originates from the different interlayer spacing of fluorographene specified for the LBTE calculation of 2D materials. The interlayer spacing designated in Cepellotti et al.[16] is 3.13 Å, almost twice smaller than that of our work 5.96 Å, as well as than the previously reported values.[32,36] In consequence, they yielded the lattice thermal conductivity ~260 W m^{-1} K^{-1} at 300 K, nearly twice larger than our result of 145.2 W m^{-1} K^{-1}. In fact, if we apply the interlayer spacing of Cepellotti et al. to our LBTE calculation, we obtain the lattice thermal conductivity 269.2 W m^{-1} K^{-1}. Therefore, our calculation result for monolayer fluorographene embodies the same physics as the results from Cepellotti et al.,[16] despite using a different experimental value for interlayer spacing to represent our work.

4. Contribution of phonon polarization

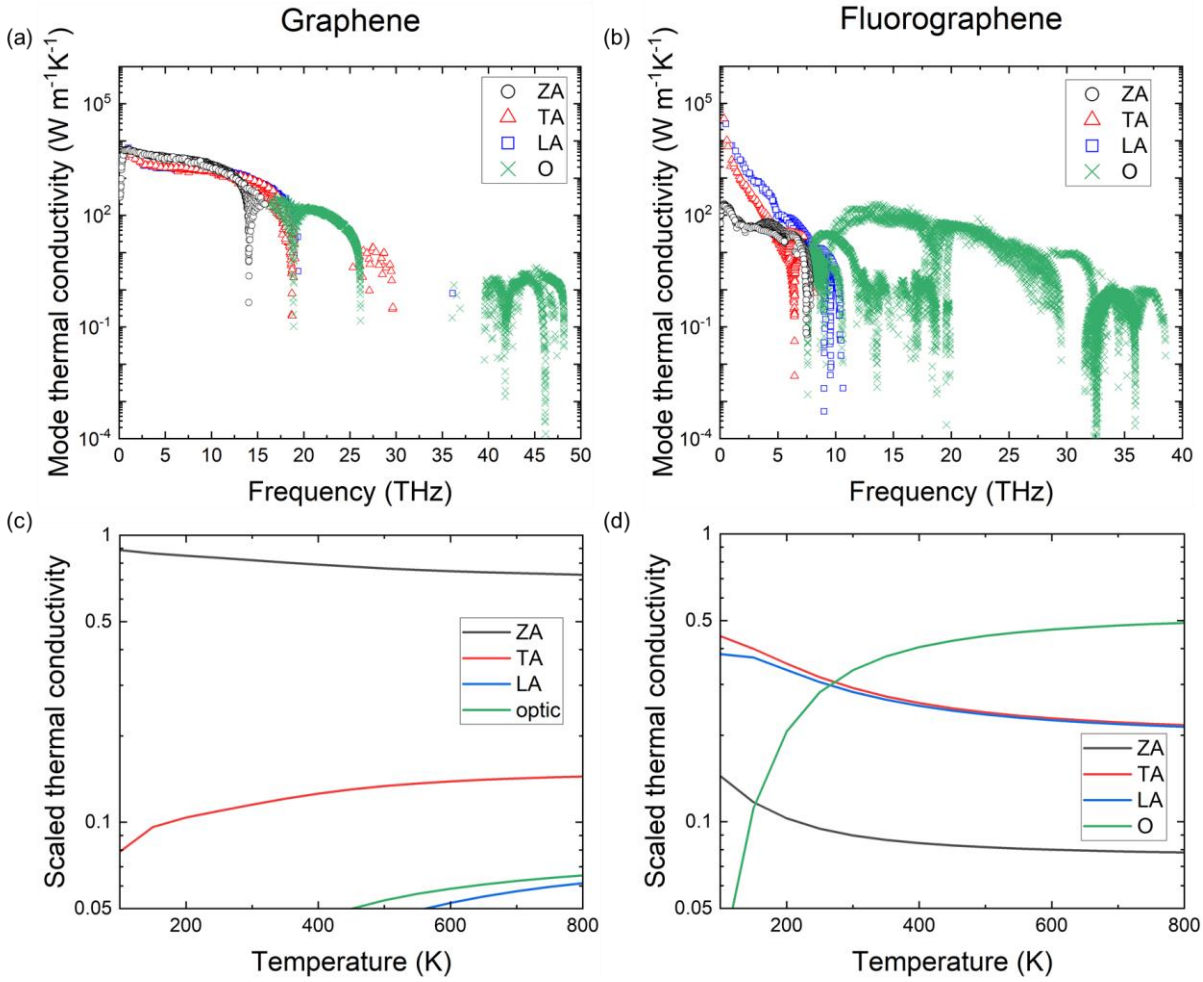

Figure 4. Mode thermal conductivity of (a) monolayer graphene and (b) fluorographene at 300K, where the full BTE is calculated with direct diagonalization of the phonon collision matrix. The scaled thermal conductivity in terms of the contribution of each phonon branch, as a function of temperature, of (c) graphene and (d) fluorographene.

We discerned the vibrational polarization of each phonon to find the role of specific phonon branches in the total thermal transport phenomena. Figure 4 shows the branch-specific mode thermal conductivity of the two materials in the full BTE solution at 300 K. All mode-dependent lattice thermal conductivities of 884 irreducible q-points are plotted in Figure 4(a-b). The contribution of each branch is summed up and normalized by the total lattice thermal conductivity in Figure 4(c-d). It is shown that over 80% of thermal transport in monolayer graphene at 300 K is contributed by the ZA phonons, which coincides with the previous report.[37] On the other hand, the contribution of ZA modes are below 10% in monolayer fluorographene at the same temperature. Here, the contribution of each of TA, LA, and optical modes is nearly 30%, respectively, and the optical modes dominate the thermal transport at the same or higher temperatures. The participation ratio of each phonon branch is completely different in monolayer graphene and fluorographene, and this difference should be thoroughly inspected to find the origin of low lattice thermal conductivity of monolayer fluorographene.

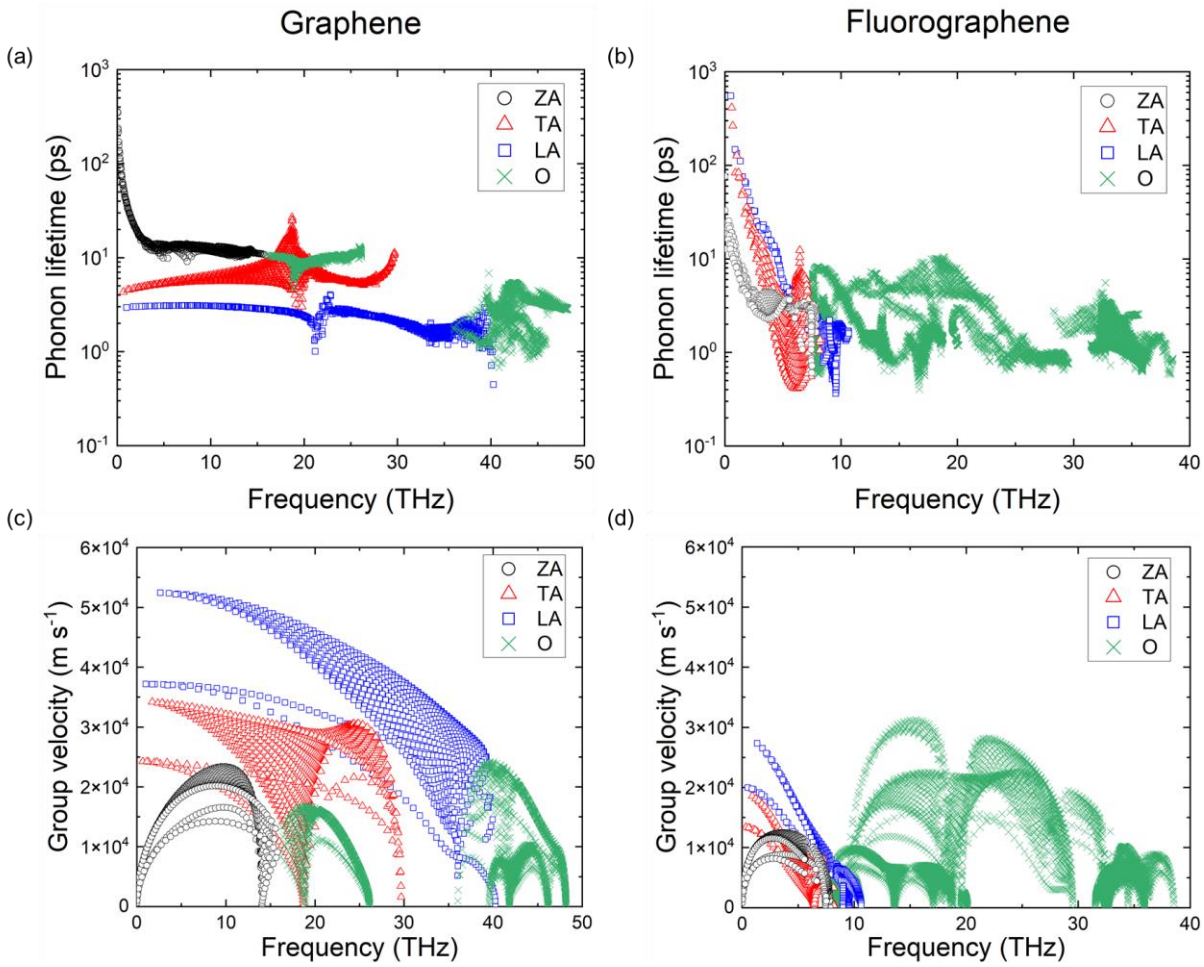

Figure 5. (a-b) Single-mode phonon lifetime and (c-d) phonon group velocities of each phonon mode in (a, c) monolayer graphene and (b, d) fluorographene.

We claim that the difference in lattice thermal conductivity in these two monolayer systems is attributed to both the phonon lifetime and group velocities. Figure 5 represents the single-mode phonon lifetime and group velocities of the 884 irreducible q-meshed phonon modes in monolayer graphene and fluorographene, respectively. For the single-mode phonon lifetime, the largest dissimilarity between the two systems are the ZA phonons near the Γ point. The lifetime of these phonons is one to two order smaller in monolayer fluorographene, compared to

graphene. It has been reported that the in-plane mirror symmetry of monolayer graphene closes off 60% of all three-phonon scattering channels involving the ZA phonon modes.[37] In monolayer fluorogrpahene, the in-plane buckling breaks this mirror symmetry and opens up all the forbidden scattering channels, increasing the scattering rate and decreasing the phonon lifetime. Thus, the broken symmetry due to the newly added fluorine atoms drastically deteriorates the lattice thermal conductivity of monolayer fluorographene.

One may inquire about the large lifetimes of the in-plane acoustic (LA and TA) phonons near 0 THz in monolayer fluorographene (Figure 5(b)), which are even larger than those in monolayer graphene (Figure 5(a)). Due to the buckled lattice structure of fluorographene, the vibrational directions of normal modes, or the eigenvectors of the dynamical matrices, are neither strictly in-plane nor out-of-plane. The in-plane acoustic normal modes, thus, partly include out-of-plane direction vibration, containing the ZA-like phonon lifetime near the zone center. However, at this ultralow frequency region near 0 THz, the number density of the TA and LA phonons is extremely smaller than that of the ZA phonons.[37] Therefore, the large single-mode phonon lifetime of the in-plane acoustic phonon modes near the Γ point cannot improve the lattice thermal conductivity of monolayer fluorographene.

With respect to the group velocities of phonons, monolayer fluorographene exhibits lower group velocity in all frequency regions than graphene does, which also contributes to the low lattice thermal conductivity. Comparison between the acoustic phonons near the zone center (the long wavelength limit) in each material system reveals that the group velocity of all modes in monolayer fluorographene decreases by nearly 50% compared to that of graphene. The same tendency applies for all acoustic phonon modes away from the Γ points, allowing us to effectively presume that the group velocities of the acoustic phonon modes of fluorographene are nearly half of those of graphene in all frequency range. This result is in line with the elastic continuum theory, which estimates the speed of sound as:[38]

$$v \sim \sqrt{\frac{K}{\rho}} \sim \sqrt{\frac{|\Phi|_{\mathrm{C-C}}}{\rho_{\mathrm{in-plane}}}},$$

where K is the bulk modulus of the solid and ρ is the equilibrium mass density. Since the second-order force constant is proportional to the bulk modulus, we can replace the bulk modulus and density with the in-plane second-order force constant $|\Phi|_{\mathrm{C-C}}$ obtained from the DFT calculation and planar density $\rho_{\mathrm{in-plane}}$, respectively, to qualitatively analyze the speed of sound in the continuum limit. By using the relevant values in Table I, the speeds of sound in graphene and fluorographene show a ratio of v_{graphene}:$v_{\mathrm{fluorographene}}$ =1:0.48, showing the same tendency as the group velocities of the acoustic phonon modes in the long wavelength limit. This analysis shows that the weak in-plane chemical bonds and large planar mass density lead to lower group velocities for the acoustic phonons, providing partial evidence of the lattice thermal conductivity in monolayer fluorographene much lower than graphene.

To fully understand the phonon group velocities, the optical phonon modes of monolayer fluorographene should also be considered since the optical modes have a dominant role in conveying heat (Figure 4(d)). In fact, certain optical branches present significantly larger group velocities than the acoustic modes in fluorographene, as shown in the 10-30 THz frequency range in Figure 5(d). These highly contributing optical modes are also noticeable by the large dispersions in the sixth and seventh phonon bands. In Figure 6(a), we plotted the phonon dispersion along the Γ-M direction and colored the phonon modes according to their mode thermal conductivity values. It appears obvious that the phonons belonging to the sixth and seventh phonon bands (or the third and fourth optical branches) feature large phonon group velocity and large mode thermal conductivity. In fact, these two branches, exhibiting 9.27 THz at the Γ point, are the only optical branches that show significant contribution to the lattice thermal conductivity. These selected optical phonon branches may be thought as important signatures of the peculiar thermal transport phenomena in functionalized graphene systems.

In-depth analysis on the high-group-velocity optical phonon modes may provide insight on the peculiar vibrational properties and thermal transport properties of fluorographene. Lindsay and Kuang[18] suggested that the large group velocities of the optical phonons in functionalized monolayer graphene emerge from the heavy atoms attached to the carbon plane. They claimed that the frequencies at the Γ point of certain phonon modes significantly

decreases as heavier atoms are attached, and the frequencies at the M point remains unchanged, resulting in steeper phonon dispersion and larger group velocity.[18] The high-group-velocity optical phonons in fluorographene, as seen in Figures 2(b) and 6(a), seem to be the case of their argument. To further understand their physical origin, we visualized the vibrational modes in the Γ-M direction of selected lower-energy optical phonons in Figures 6(b-e). In the two lowest-frequency optical modes, 7.53 THz at the Γ point, the carbon atoms comprising the 2D plane remains nearly stationary, and only the fluorine atoms vibrate in the opposite direction (Figures 6(b-c)). However, in the next two optical branches, or the high-group-velocity optical branches, the carbon atoms vibrate in phase to each other (Figures 6(d-e)). Since these selected optical branches of monolayer fluorographene originate from the zone-folded TA (Figure 6(d)) and LA (Figure 6(e)) branches of graphene, they tend to exhibit larger group velocities and can dominantly contribute to the overall thermal transport process, despite much smaller lattice thermal conductivity than that of monolayer graphene. This result suggests that the changes in the phonon structure arisen by functionalization can be traced back by examining the phonon polarization.

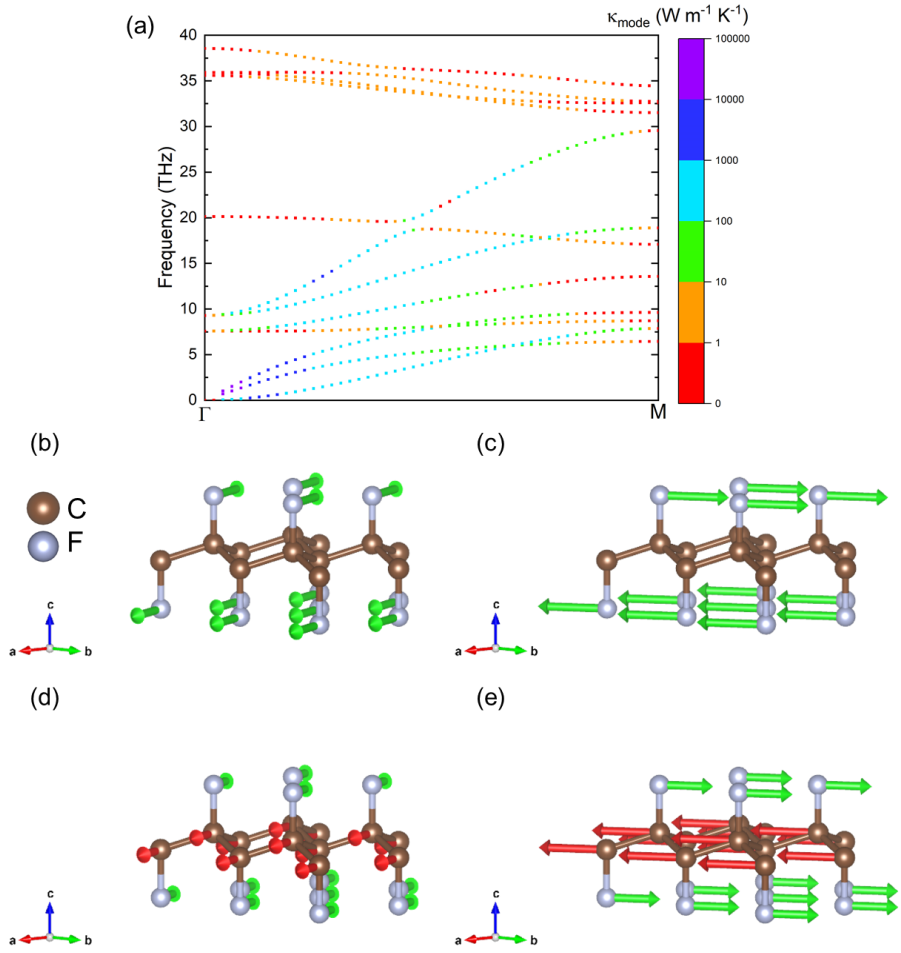

Figure 6. (a) Phonon dispersion along the Γ-M direction with respective phonon modes colored according to the mode thermal conductivity, where the range of mode thermal conductivity is indicated in the color bar on the right. (b-e) Schematics of the vibration modes of the first four optical modes (or (b) the fourth, (c) fifth, (d) sixth, and (e) seventh phonon bands) near the Γ point. Their frequencies at the Γ point are (b) 7.53, (c) 7.53, (d) 9.27, and (e) 9.27 THz, respectively. The red (green) arrows illustrate the eigenvector of the dynamical matrix corresponding to the carbon (fluorine) atoms. For the phonon modes along the Γ-M direction, the lattice vibrates in response to the incident (q_x, 0, 0) momentum, whose direction is parallel to the $\mathbf{b}_1$ reciprocal lattice vector of Figure 1(c). Phonon modes (b) and (d) exhibit transverse-like polarization, and (c) and (e) longitudinal-like.

IV. Conclusion

This work investigated the phonon transport in fluorographene, the electrically insulating derivative to monolayer graphene. We performed DFT and DFPT calculation and exactly solved the phonon Boltzmann transport equation in order to find the origin of the suppressed lattice thermal conductivity of monolayer fluorographene and the peculiarity in its phonon structures. The lattice thermal conductivities of infinitely large samples are 2,868.6 and 145.2 W m^{-1} K^{-1} for monolayer graphene and fluorographene at 300 K, respectively, showing twenty-time difference. On the other hand, the thermal conductivity of finite-size systems implies that fluorographene is less affected by the system size than graphene, which can be advantageous for nanoscale thermal management, in addition to the electrically insulating characteristic. Further investigation of the polarization-dependent intrinsic phonon properties, the phonon group velocities, and lifetimes provided direct evidence of the correlation between the structural properties of monolayer fluorographene and its relatively low lattice thermal conductivity. Through systematic comparison with monolayer graphene, we concluded that both short phonon lifetime and low phonon group velocities of fluorographene contributes to the twentyfold lower thermal conductivity. Here, the broken mirror symmetry reduces the ZA phonon lifetime, and the weak in-plane bond strength and large mass density halves the group velocity of all acoustic phonons. Analysis on the optical phonon modes revealed that certain optical phonon branches in fluorographene are, in principle, derived from the zone-folded in-plane acoustic modes in graphene and turned out to have dominating contribution to the total thermal transport process. Our analysis of the intrinsic phonon properties based on the vibration polarization of each phonon mode provided a means to correlate the influence of functionalization to the phonon structure. We expect that the approach of this research may also be utilized to study the thermal transport properties of other graphene-derived materials. This may facilitate the discovery of new 2D thermal management material by engineering the functional groups of graphene.

1 W. Cai, A. L. Moore, Y. Zhu, X. Li, S. Chen, L. Shi, and R. S. Ruoff, Nano Letters **10,** 1645 (2010).
2 A. A. Balandin, S. Ghosh, W. Bao, I. Calizo, D. Teweldebrhan, F. Miao, and C. N. Lau, Nano Letters **8,** 902 (2008).
3 J.-U. Lee, D. Yoon, H. Kim, S. W. Lee, and H. Cheong, Physical Review B **83,** 081419 (2011).
4 L. Lindsay, D. A. Broido, and N. Mingo, Physical Review B - Condensed Matter and Materials Physics **83,** 235428 (2011).
5 P. Huang, Y. Li, G. Yang, Z.-X. Li, Y.-Q. Li, N. Hu, S.-Y. Fu, and K. S. Novoselov, Nano Materials Science **3,** 1 (2021).
6 Y. Fu, J. Hansson, Y. Liu, S. Chen, A. Zehri, M. K. Samani, N. Wang, Y. Ni, Y. Zhang, Z.-B. Zhang, Q. Wang, M. Li, H. Lu, M. Sledzinska, C. M. S. Torres, S. Volz, A. A. Balandin, X. Xu, and J. Liu, 2D Materials **7,** 012001 (2020).
7 D. Mani, M. C. Vu, T.-H. Jeong, J.-B. Kim, C.-S. Lim, J.-H. Lim, K.-M. Kim, and S.-R. Kim, Composites Part A: Applied Science and Manufacturing **149,** 106585 (2021).
8 M. C. Vu, I.-H. Kim, W. K. Choi, C.-S. Lim, M. A. Islam, and S.-R. Kim, ACS Applied Materials & Interfaces **12,** 26413 (2020).
9 D. K. Nguyen, T. T. H. Tran, T. K. L. Mai, M.-S. Tran, S. Ghotekar, A. L. H. Pham, V.-C. Nguyen, and M. C. Vu, ACS Applied Nano Materials **7,** 2724 (2024).
10 J. Huo, G. Zhang, X. Zhang, X. Yuan, and S. Guo, ACS Applied Materials & Interfaces **15,** 52984 (2023).
11 X. Wang and P. Wu, ACS Applied Materials & Interfaces **11,** 21946 (2019).
12 R. Zbořil, F. Karlický, A. B. Bourlinos, T. A. Steriotis, A. K. Stubos, V. Georgakilas, K. Šafářová, D. Jančík, C. Trapalis, and M. Otyepka, Small **6,** 2885 (2010).
13 K.-J. Jeon, Z. Lee, E. Pollak, L. Moreschini, A. Bostwick, C.-M. Park, R. Mendelsberg, V. Radmilovic, R. Kostecki, T. J. Richardson, and E. Rotenberg, ACS Nano **5,** 1042 (2011).
14 W. Huang, Q. X. Pei, Z. Liu, and Y. W. Zhang, Chemical Physics Letters **552,** 97 (2012).
15 G. Fugallo, A. Cepellotti, L. Paulatto, M. Lazzeri, N. Marzari, and F. Mauri, Nano Letters **14,** 6109 (2014).
16 A. Cepellotti, G. Fugallo, L. Paulatto, M. Lazzeri, F. Mauri, and N. Marzari, Nature Communications **6,** 1 (2015).
17 M. C. Vu, N. A. Thi Thieu, J.-H. Lim, W.-K. Choi, J. Chan Won, M. A. Islam, and S.-R. Kim, Carbon **157,** 741 (2020).
18 L. Lindsay and Y. Kuang, Physical Review B **95,** 121404 (2017).
19 G. Kresse and J. Furthmüller, Physical Review B **54,** 11169 (1996).
20 J. P. Perdew, K. Burke, and M. Ernzerhof, Physical Review Letters **77,** 3865 (1996).

[21] G. Kresse and D. Joubert, Physical Review B **59,** 1758 (1999).
[22] O. Leenaerts, H. Peelaers, A. D. Hernández-Nieves, B. Partoens, and F. M. Peeters, Physical Review B - Condensed Matter and Materials Physics **82,** 195436 (2010).
[23] Y. X. Zhao and I. L. Spain, Physical Review B **40,** 993 (1989).
[24] A. Togo, Journal of the Physical Society of Japan **92** (2022).
[25] F. Eriksson, E. Fransson, and P. Erhart, Advanced Theory and Simulations **2,** 1800184 (2019).
[26] W. Li, J. Carrete, N. A. Katcho, and N. Mingo, Computer Physics Communications **185,** 1747 (2014).
[27] W. Li, L. Lindsay, D. A. Broido, D. A. Stewart, and N. Mingo, Physical Review B **86,** 174307 (2012).
[28] A. Togo, L. Chaput, and I. Tanaka, Physical Review B - Condensed Matter and Materials Physics **91,** 094306 (2015).
[29] L. Chaput, Physical Review Letters **110,** 265506 (2013).
[30] A. Cepellotti and N. Marzari, Physical Review X **6,** 041013 (2016).
[31] P. E. Blöchl, O. Jepsen, and O. K. Andersen, Physical Review B **49,** 16223 (1994).
[32] H. Touhara, K. Kadono, Y. Fujii, and N. Watanabe, Zeitschrift für anorganische und allgemeine Chemie **544,** 7 (1987).
[33] N. Mounet and N. Marzari, Physical Review B - Condensed Matter and Materials Physics **71,** 205214 (2005).
[34] H. Peelaers, A. D. Hernández-Nieves, O. Leenaerts, B. Partoens, and F. M. Peeters, Applied Physics Letters **98,** 051914 (2011).
[35] A. Ward and D. A. Broido, Physical Review B **81,** 085205 (2010).
[36] S. S. Han, T. H. Yu, B. V. Merinov, A. C. T. Van Duin, R. Yazami, and W. A. Goddard, Chemistry of Materials **22,** 2142 (2010).
[37] L. Lindsay, D. A. Broido, and N. Mingo, Physical Review B - Condensed Matter and Materials Physics **82,** 115427 (2010).
[38] J. M. Ziman, *Electrons and phonons : the theory of transport phenomena in solids* (Oxford: Oxford University Press, Oxford, 2001).